Electromagnetic radiation from strong Langmuir turbulence

K. Akimoto
Earth and Space Science Division and Applied Theoretical Division, Los Alamos National Laboratory, Los Alamos, New Mexico 87545

H. L. Rowland[a] and K. Papadopoulos
Department of Physics and Astronomy, University of Maryland, College Park, Maryland 20742

(Received 6 July 1987; accepted 18 April 1988)

A series of computer simulations is reported showing the generation of electromagnetic radiation by strong Langmuir turbulence. The simulations were carried out with a fully electromagnetic $2\frac{1}{2}$-dimensional fluid code. The radiation process takes place in two stages that reflect the evolution of the electrostatic turbulence. During the first stage while the electrostatic turbulence is evolving from an initial linear wave packet into a planar soliton, the radiation is primarily at ω_e. During the second stage when transverse instabilities lead to the collapse and dissipation of the solitons, $2\omega_e$ and ω_e radiation are comparable, and $3\omega_e$ is also present. The radiation power at $\omega = 2\omega_e$ is in good agreement with theoretical predictions for electromagnetic emissions by collapsing solitons.

I. INTRODUCTION

Theoretical[1–3] and experimental[4–7] results have convincingly demonstrated that the description of Langmuir turbulence as an ensemble of weakly interacting plasmons is not applicable to most laboratory and astrophysical plasmas. The ponderomotive force due to Langmuir waves excited by electron beams or other means creates regions of lower plasma density (cavitons) where the high frequency Langmuir waves are trapped. The localized Langmuir wave packets (solitons) have energy densities several orders of magnitude higher than the average energy density and are extremely dynamic. The caviton–soliton pairs are centers of electromagnetic (em) radiation near the plasma frequency and its harmonics.[4,5] The em radiation is a key diagnostic signature of the processes occurring in many space and astrophysical plasmas permeated by energetic electron beams.

Early theories on the emission relied on weak turbulence conversion of Langmuir to em waves. Such theories and their diagnostic interpretation are invalid for most of the relevant space and laboratory situations. Recent analytic theories considered some of the localized aspects of the strong Langmuir turbulence in the calculation of the em emission.[8–12] However, the dynamic nature of the caviton–soliton turbulence and the lack of an expansion parameter in the strong turbulence regime makes the analysis suspect.

It is the purpose of this paper to present the results from a $2\frac{1}{2}$-dimensional ($2\frac{1}{2}$-D) fully em two fluid code which was especially constructed to study dynamically the em emission processes under conditions of strong turbulence. It should be noted that the use of the Zakharov equations is not appropriate for the problem because of the averaging of the high frequency fields, while particle simulations cannot accommodate the number of particles per Debye length required to reduce the effect of numerical noise on the radiation development and absorption. For this reason we developed an em version of a two fluid code. The electrostatic version of this code was previously used to study the properties of Langmuir soliton–caviton pairs for magnetized and unmagnetized plasmas.[13] It should be noted that Pritchett and Dawson[14] performed $2\frac{1}{2}$-D particle simulations of the conversion of electron beam generated plasma waves to em waves. The simulation parameters, the ion model, and the temperature ratio ($T_e/T_i \approx 20$) were such that the weak turbulence conversion of Langmuir waves by fixed ion density fluctuations or by large amplitude sound waves was dominant. They, however, were not able to extend the results into the strong turbulence regime.

II. COMPUTATIONAL MODEL AND RESULTS

The simulation code is a fully nonlinear $2\frac{1}{2}$-D em two fluid code. It solves by a finite difference scheme the following fluid and Maxwell's equations:

$$\frac{\partial n_j}{\partial t} = -\nabla(n_j \mathbf{v}_j),$$

$$\frac{\partial \mathbf{v}_j}{\partial t} = -(\mathbf{v}_j\cdot\nabla)\mathbf{v}_j + \frac{q_j}{m_j}\left(E + \frac{1}{c}\mathbf{v}_j \times \mathbf{B}\right) - \frac{\nabla P_j}{m_j n_j} - \nu_j \mathbf{v}_j,$$

$$\frac{\partial \mathbf{B}}{\partial t} = -c\nabla\times\mathbf{E},$$

$$\frac{\partial \mathbf{E}}{\partial t} = c\nabla\times\mathbf{B} - \mathbf{J},$$

where $P_j = \gamma_j n_j T_j$, with $j = e$ and i electrons for ions, respectively. The ratio of specific heats used here was $\gamma_e = 3$ and $\gamma_i = 1$. This guarantees that both the low and high frequency modes have the correct linear dispersion. The temperatures are assumed constant. Based upon earlier simulations,[13,15] until the collapse takes place there is no heating of the background plasma. When the collapse occurs, the electrons are heated by the formation of superthermal tails. An effective collision frequency $\nu_j/\omega_e = \alpha_j(k\lambda_D)^6 + \beta_j(k\lambda_D)^2$ which simulates collisionless Landau-type damping, was used with $\alpha_e = 1$, $\beta_e = 0.0$, $\alpha_i = 1$, and $\beta_i = 10^{-3}$ (ω_e is the plasma frequency and λ_D is the Debye length).

[a] Present address: Naval Research Laboratory, Washington, D.C. 20375-5000.

 0031-9171/88/082185-05$01.90

We present below the results of a rather typical run which highlights many of the important *dynamic* features of the conversion process. The computations were performed in the x-y plane of a doubly periodic 64×64 system with cell size $\Delta x=\Delta y=10^{1/2}\lambda_D$. The system was initialized with a Langmuir wave pocket whose ω and k satisfied the linear dispersion relation $\omega^2=\omega_e^2+3k^2v_e^2$, where v_e is the electron thermal speed. The wave packet contained three modes (3,0) and (3, $\pm$ 1). The mode (3,0) contained 80% of the energy, while the rest was equally shared by the other two modes. The spectrum was chosen to model the turbulence that would be generated by a warm electron beam streaming in the positive x direction. The turbulence parameter $\overline{W}\equiv E^2/4\pi n_0T_e$, where E is the amplitude of the Langmuir wave, and n_0 and T_e the ambient plasma density and temperature, was taken as $\overline{W}=0.2$. For the mass ratio used ($m_e/M_i=10^{-2}$) and the corresponding value of $k_0\lambda_e=0.09$, where k_0 corresponds to mode (3,0), the system was in the strong turbulence regime, $\overline{W}>(k\lambda_e)^2$, m_e/M_i. The value of c/v_e was 12.65 and $T_e=T_i$.

The general evolution of the initial linear wave packet is in good agreement with the one observed in the earlier purely electrostatic simulations.[13] At $50\omega_e^{-1}$, the initial wave packet becomes slightly modulated and evolves into three soliton–caviton pairs at $\omega_et=100$. These are planar solitons with their transverse dimension determined by the transverse width of the linear wave packet. Because the initial spectrum was chosen to model the waves driven by a warm electron beam, it is strongly aligned in one direction. The solitons form in the direction of the initial electrostatic (es) fields. At $200\omega_e^{-1}$, the transverse fields begin to grow. The local es field energy reaches its maximum at approximately $\omega_et=300$, while the cavity reaches its minimum slightly later. Figures 1 and 2 show the two-dimensional spatial profiles of the es energy and of the ion density at $\omega_et=300$ averaged over $50\omega_e^{-1}$. The collapse was observed to be slightly subsonic. The es field energy was rapidly dissipated and the solitons were virtually nonexistent by $\omega_et=500$ while the cavities were still present but were converting to ion waves. The soliton–caviton pairs at this stage are sometimes called burnouts. It is well known that most of the dissipated wave energy heats the electrons by the formation of superthermal tails.[6,13]

Figure 3 shows the time history of the total wave energy and the em field energy, normalized to the thermal energy. The total energy stays approximately constant until $\omega_et=200$. Then the dissipation proceeds quite rapidly with 40% of the wave energy damped in $50\omega_e^{-1}$ about $\omega_et=300$.

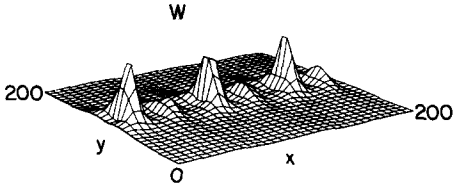

FIG. 1. Spatial distribution of time averaged es field energy at $t=300\omega_e^{-1}$ showing the presence of solitons. The vertical scale is linear with $W_{es,max}=2.15$.

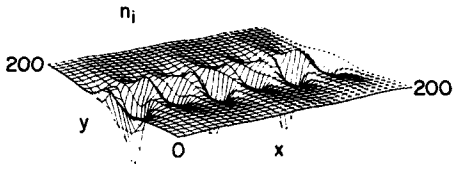

FIG. 2. Ion density distribution at $t=300\omega_e^{-1}$ showing the presence of cavitons. The vertical scale is linear with $(\delta_n/n_0)_{min}=0.5$.

The planar solitons which first form stabilize at long enough wavelengths so that there is little coupling to the heavily damped short wavelength modes. During the formation of the planar solitons there is a small enhancement of the em field energy. With the collapse of the solitons, the em fields grow by three orders of magnitude until the es energy dissipates. The total radiation reaches its maximum energy at $t\simeq300\omega_e^{-1}$ which is also when the es energy reaches its largest local maximum. Even though the total es energy is dropping, the strong turbulence acts to compress the remaining field energy so that the most intense local fields occur at $t=300\omega_e^{-1}$ with $W=2.15$. At this time 7% of the initial wave energy has been converted into em energy.

Figure 3 shows that the growth of em field energy occurs in two stages. To see this process in more detail we also calculated the power ($\equiv\partial W/\partial t$) in three frequency bands around ω_e, $2\omega_e$, and $3\omega_e$. This is shown on Fig. 4. The power was calculated by first summing the energy in three separate regions of the k space spectrum of W_{em} at each time step. These regions were determined from the linear dispersion for the em waves with region 1 for $\omega_e<\omega<1.3\omega_e$, region 2 for $1.6\omega_e<\omega<2.3\omega_e$, and region 3 for $2.6\omega_e<\omega<3.3\omega_e$. The width of these bands was determined from the spectral width seen in the Fourier transform of the em field at individual grid points. The field energy was averaged for 15 time steps ($3\omega_e^{-1}$). The average from the previous $3\omega_e^{-1}$ period was subtracted and the difference was divided by $3\omega_e^{-1}$. Therefore P is normalized to $nT_e\omega_e$. Since we are interested in times of positive growth of the em field and also need to plot the data on a semilogarithmic scale to cover the dynamic range, the plotted P is the larger of P or 10^{-10}. The gaps seen on Fig. 4 at late times simply reflect that $\partial W_{em}/\partial t<0$ as can be seen in Fig. 3. Most of the time one sees high frequency fluctuations in P. These are due to small fluctuations in W_{em}. However, one can clearly identify two periods of sustained positive P which are associated with the two periods of growth in W_{em} seen in Fig. 3. The first burst of radiation, which occurs when the planar solitons form, is at ω_e. One sees that $P(\omega_e)\gg P(2\omega_e)$ until $\omega_et=200$. When the solitons

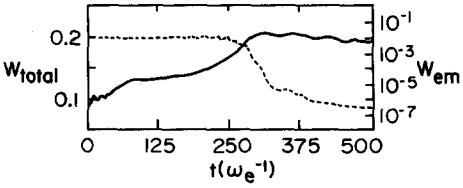

FIG. 3. Time history of the total field energy (dotted line) and the em field energy (solid line). Note the different vertical scales.

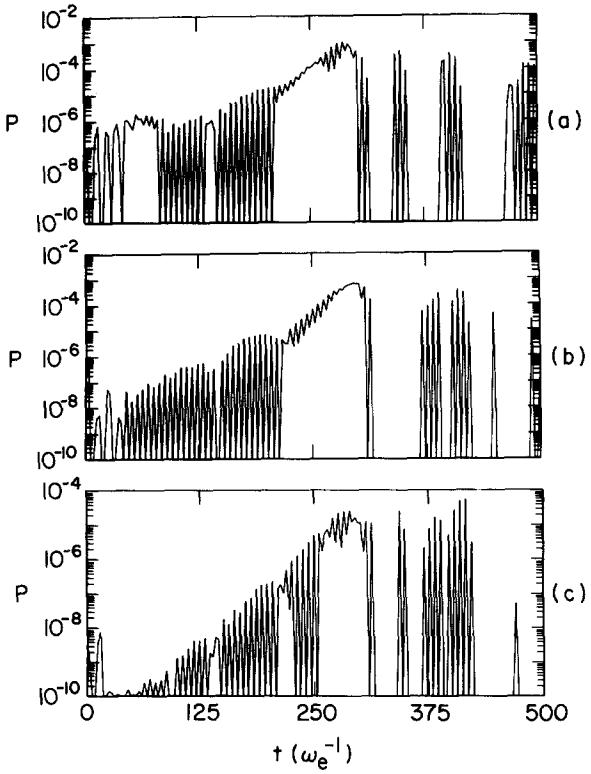

FIG. 4. Time history of em power densities of ω_e, $2\omega_e$, and $3\omega_e$ [(a), (b), and (c), respectively].

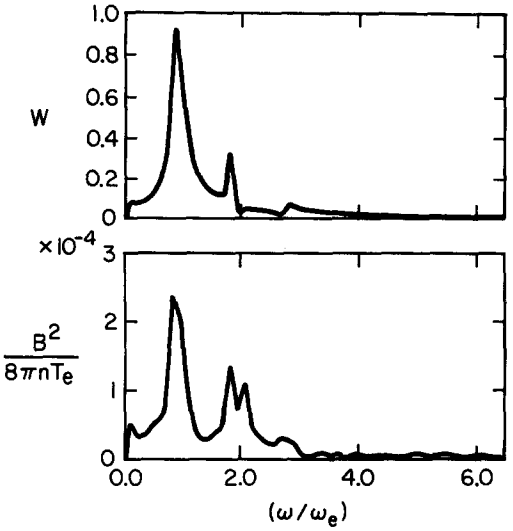

FIG. 5. Frequency spectrum for the electrostatic turbulence (W) and magnetic field energy at $t = 350\omega_e^{-1}$.

are fully developed at $\omega_e t = 300$, $P(\omega_e) \simeq P(2\omega_e)$, and a significant level of $3\omega_e$ is observed. The radiation field decreases at late times ($\omega_e t > 300$) mainly because of a reverse conversion of ω_e em waves to Langmuir waves. This change between early and late times is also seen in the radiation pattern. During the early stages when the ω_e emission is dominant, the radiation has a dipole pattern. The largest modes in the k-space spectrum of the em field energy are $(0, +1)$ and $(0, -1)$. At $300\omega_e^{-1}$, following the growth of the $2\omega_e$ radiation, one sees in addition to the dipole fluid two quadrupole spectra: the $2\omega_e$ spectrum at $(\pm 3, \pm 3)$ and the $3\omega_e$ spectrum at $(\pm 6, \pm 4)$. These results are consistent with theoretical predictions.[10–12] An important effect can be seen from Fig. 5. At $\omega_e t \geqslant 350$ the spectral peaks for both the es and em waves show substantial broadening. The broadening seems consistent with nonlinear frequency shifts caused by strong turbulence $\Delta\omega \sim \omega_e \overline{W}_{\max}$. Broadening of the radiation spectrum has been observed experimentally by Cheung *et al.*[5]

III. CONVERSION PHYSICS

In the preceding section, we have discussed the radiation process in terms of spatially averaged quantities such as field energies and radiation densities. As can be seen from Fig. 1, strong turbulence leads to localized structures. Figure 6 shows the total es field energy at $\omega_e t = 300$ for the center of the simulation grid. The total grid covers (0 to 200)λ_D in both the x and y directions. This is the middle soliton seen in Fig. 1. Figure 7 plots the normalized E_y^2 es field at $\omega_e t = 300$. The maximum E_y^2 is approximately an order of magnitude less than the maximum E_x^2 field. One can see that at the center of the soliton, it is a basically one-dimensional structure with the es field in the x direction. Figure 8 shows the normalized B_z^2. Figure 9 is the current vorticity. The local current vorticity $\nabla \times \mathbf{J}$ is the source of the em emission as expected on the basis of the wave equation

$$\nabla^2 \mathbf{B} - \frac{1}{c^2}\frac{\partial \mathbf{B}}{\partial t} = \frac{\nabla \times \mathbf{J}}{c}.$$

By examining these diagnostics it is easy to see the emission source regions are not located at the center of the solitons where the es energy density maximizes but at the edges. In fact, the source regions correlate well with regions where the E_y component of the es field maximizes. This is consistent with the results of Ref. 11, which indicate that the conversion efficiency to em radiation scales with the transverse to longitudinal soliton aspect ratio and the electrostatic to electromagnetic coupling disappears in the limit of zero aspect ratio. This has important implications with respect to the time dependence of em emissions during beam–plasma interactions. In this case the es wave spectrum is mainly one dimensional with k parallel to the beam velocity. This leads to the formation of planar solitons during which time the em emission is very weak. Strong em emission is produced during the next stage of transverse collapse which increases the soliton aspect ratio. Most of the emission is localized at the edges of the soliton where the es field curvature and the

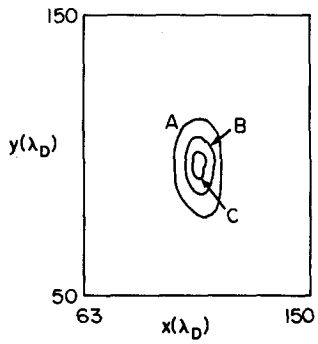

FIG. 6. Linear contour plot of the total es field energy at $t = 300\omega_e^{-1}$. This is the middle soliton shown in Fig. 1. Full mesh covers (0 to 200)λ_D in both x and y. Here $C = 1.8$ and $A = 0.35$.

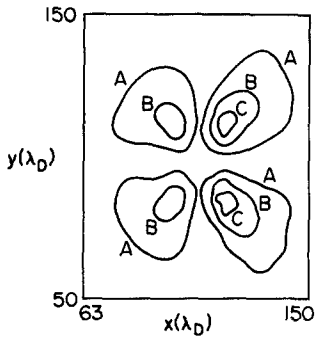

FIG. 7. The $E_y^2/4\pi nT_e$ es field energy at $t=300\omega_e^{-1}$. Here $C=9.67\times10^{-2}$ and $A=1.93\times10^{-2}$.

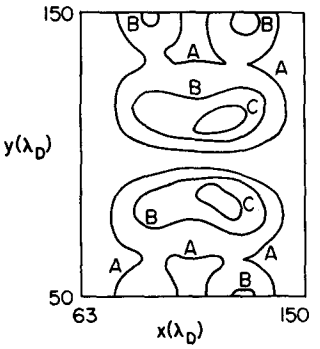

FIG. 8. The $B_z^2/4\pi nT_e$ at $t=300\omega_e^{-1}$ showing the correlation with E_y^2. Here $C=5.77\times10^{-3}$ and $A=1.15\times10^{-3}$.

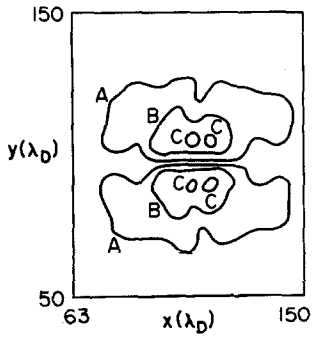

FIG. 9. Radiation source term $(\nabla\times j)$ at $300\omega_e^{-1}$. Soliton radiation is from the sides, not the center. There is a mixture of dipole and quadrupole radiation. Here $C=1.56\times10^{-2}$ and $A=3.12\times10^{-3}$.

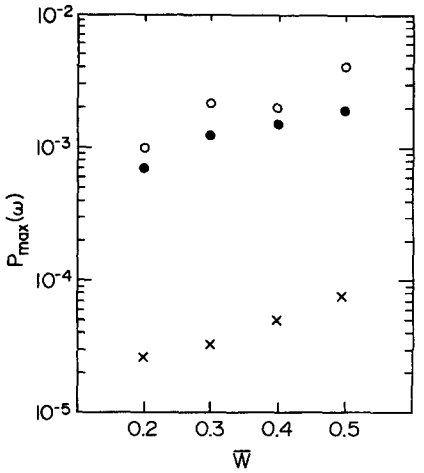

FIG. 10. Radiation power density versus initial es turbulence for ω_e, $2\omega_e$, and $3\omega_e$ (open circle, closed circle, and $\times$, respectively).

transverse part of the es field maximize. Equivalent mode coupling descriptions can also be seen in the code by looking at individual Fourier components. For example, the $2\omega_e$ radiation is consistent with coupling of the $(\pm3,\pm2)$ and $(\pm3,\pm3)$ modes with $(0,\pm1)$ and (0,0) modes. The Langmuir waves with large k_y grow because of the transverse modulational instability.

The maximum radiation power densities obtained in the simulation can be compared with a weak turbulence theory[14] and the strong turbulence theory of Freund and Papadopoulos.[11,12] We use Eqs. (13) and (14a) of Ref. 14 to estimate the power density emitted at $\omega\sim\omega_e$:

$$P(\omega)=\frac{1}{24\pi^2}\left(\frac{v_e}{c}\right)^3\left(\frac{\delta n}{n}\right)^2\left(\frac{k}{\Delta k}\right)\left(\frac{\lambda_i}{\lambda_D}\right)^2\times\int(\omega^2-1)^{1/2}W_{es}(\omega)d\omega,$$

where $\omega_e\equiv1$, $(\delta n/n)$ is the average ion density fluctuations, and $(k_i/\Delta k)$ is the ratio of the typical ion wavenumber to the spectral bandwidth, $\lambda_i=2\pi/k_i$. To obtain an estimate of P one can assume $W_{es}(\omega)=\bar{W}_0\delta(\omega-\omega_0)$, where $\omega_0^2=1+3k^2\lambda_D^2$ and $\bar{W}_0$ is the average es field energy. For this simulation $c/v_e=12.64$, $k_i/\Delta k\simeq3$, $\lambda_i/\lambda_D\simeq34$, and $k\lambda_D=0.093$. At $t=300\omega_e^{-1}$, $\bar{W}_0=0.2$ and $(\delta n/n)=4.7\times10^{-2}$. Note that these are not the local maximums or minimums but are the spatially averaged values. These are appropriate for a weak turbulence calculation since weak turbulence assumes homogeneous, uniform fluctuations. At $t=300\omega_e^{-1}$, this yields a value of $P(\omega_e)\simeq2.10^{-7}$, which is far below the observed value 10^{-3}. The power emitted by a Langmuir soliton at $\omega\sim2\omega_e$ can be computed by Eqs. (16) and (17) of Ref. 11. From this we can obtain the normalized power density at $t\sim300\omega_e^{-1}$, which is $P(2\omega_e)\sim6.1\times10^{-4}$ in good agreement with the observed value of 7×10^{-4}. The scaling of the emission with the level of turbulence $\bar{W}$ for ω_e, $2\omega_e$, and $3\omega_e$ is shown in Fig. 10. The emission scales linearly with $\bar{W}$ consistent with the results of Ref. 11.

IV. SUMMARY AND CONCLUSIONS

The results from a fully em $2\frac{1}{2}$-D two fluid simulation of em emission during soliton formation and collapse have been presented. Two sequential emission stages are observed. During the first stage, while the initial linear wave packet forms planar solitons, $P(\omega_e)\gg P(2\omega_e)$ and the radiation has a dipole pattern. During soliton collapse transverse es fields are rapidly produced around the centers of the solitons, resulting in strong harmonic emission with $P(\omega_e)\sim P(2\omega_e)$ and substantial $3\omega_e$ emission. The $2\omega_e$ and $3\omega_e$ radiation has quadrupole patterns. The total emission is several orders of magnitude stronger than expected on the basis of weak turbulence theory; in addition $P(2\omega_e)/P(\omega_e)\simeq O(1)$ rather than the $(v_e/c)^2$ scaling of weak turbulence. The analytic theory of Ref. 11, where the soliton–caviton pair was treated as static during the radiation emission, predicts the correct scaling with $\bar{W}$, the $P(2\omega_e)/P(\omega_e)=O(1)$ ratio, and the quadrupole nature of the harmonics. The per soliton emission is estimated within a factor of 2, without the dynamic aspects of the collapse. Results pertaining to scaling with

v_e/c, ion mass ratio, and the emission from a collection of solitons will be published later.

ACKNOWLEDGMENTS

One of the authors (K.A.) would like to thank Professor T. Ogino and Dr. P. L. Pritchett for valuable discussions.

This work was supported by the National Science Foundation under Grant No. ATM-85-00794, and the Office of Naval Research under Grant No. N00014-85-K-0746. The computations were carried out at the National Center for Atmospheric Research and the San Diego Supercomputer Center, which are supported by the National Science Foundation.

[1]V. E. Zakharov, in *Handbook of Plasma Physics*, edited by A. A. Galeev and R. N. Sudan (North-Holland, Amsterdam, 1984), Vol. 2, p. 81.

[2]L. I. Rudakov and V. N. Tsytovich, Phys. Rep. C **40**, 1 (1978).

[3]S. G. Thornhill and D. ter Haar, Phys. Rep. C **43**, 1 (1978).

[4]D. A. Gurnett and R. R. Anderson, Science **194**, 1159 (1976); J. Geophys. Res. **82**, 632 (1977).

[5]P. Y. Cheung, A. Y. Wong, C. B. Darrow, and S. J. Qian, Phys. Rev. Lett. **48**, 1348 (1984); P. Y. Cheung and A. Y. Wong, Phys. Fluids **28**, 1538 (1985).

[6]K. G. Kato, G. Benford, and D. Tzach, Phys. Rev. Lett. **50**, 1587 (1983); Phys. Fluids **26**, 3636 (1983).

[7]D. A. Whelan and R. L. Stenzel, Phys. Rev. Lett. **95**, 95 (1981); Phys. Fluids **28**, 958 (1985).

[8]B. N. Brejzman and L. S. Pekker, Phys. Lett. **65**, 121 (1978).

[9]M. V. Goldman, G. F. Reiter, and D. R. Nicholson, Phys. Fluids **23**, 388 (1980); B. Hafizi and M. V. Goldman, *ibid.* **24**, 145 (1981).

[10]K. Papadopoulos and H. Freund, Geophys. Res. Lett. **5**, 881 (1978).

[11]H. P. Freund and K. Papadopoulos, Phys. Fluids **23**, 732 (1980).

[12]H. P. Freund and K. Papadopoulos, Phys. Fluids **23**, 1546 (1980).

[13]H. L. Rowland, J. Lyon, and K. Papadopoulos, Phys. Rev. Lett. **46**, 346 (1981); H. L. Rowland, Phys. Fluids **28**, 190 (1985).

[14]P. L. Pritchett and J. M. Dawson, Phys. Fluids **26**, 1114 (1983).

[15]H. L. Rowland, Phys. Fluids **23**, 508 (1980).